Supplementary information

Realization and direct observation of five normal and parametric modes in silicon nanowire resonators by in situ transmission electron microscopy

Feng-Chun Hsia,[a,b,c] Dai-Ming Tang,[*a] Wipakorn Jevasuwan,[a] Naoki Fukata,[a] Xin Zhou,[a] Masanori Mitome,[a] Yoshio Bando,[a,d,e] Torbjörn E.M. Nordling,[b] Dmitri Golberg[a,f]

[a]International Center for Materials Nanoarchitectonics (MANA), National Institute for Materials Science (NIMS), 1-1 Namiki, Tsukuba, Ibaraki 305-0044, Japan

[b]Department of Mechanical Engineering, National Cheng Kung University, No.1, University Road, Tainan City 701, Taiwan

[c] Advanced Research Center for Nanolithography (ARCNL), Science Park 106, Amsterdam 1098 XG, The Netherlands

[d]Australian Institute for Innovative Materials, University of Wollongong, Wollongong, New South Wales 2500, Australia

[e]Institute of Molecular Plus, Tianjin University. No. 11 Building, No. 92 Weijin Road, Nankai District, Tianjin, 300072, P. R. China

[f]School of Chemistry, Physics and Mechanical Engineering, Science and Engineering Faculty, Queensland University of Technology (QUT), 2nd George str., Brisbane, QLD 4000, Australia

Note S1. Growth of Si NWs and structure characterization

The Si NWs employed in our experiments were synthesized on a n-type Si (111) substrate by using 3 nm gold nanoparticles as catalysts following a vapor–liquid–solid (VLS) growth. The background pressure of the CVD chamber was about 10^{-5} Pa. Si NWs were grown at 600 °C for 30 min using a 19 sccm (standard cubic centimeter per minute) flow of SiH_4, with the total pressure set to ~800 Pa by mixing SiH_4 with a nitrogen gas. Table S1 lists statistical data on structural information of the Si NWs tested in this work.

Table S1: Structural information from 10 analyzed Si NWs

Samples	Diameter (nm)	Oxide layer thickness (nm)	Length (nm)
1	43.7	0.8	1815.7
2	34.8	1.8	2898.1
3	22.9	1.9	1588.0
4	21.7	2.0	2002.7
5	23.3	0.7	2528.9
6	30.8	2.6	4783.4
7	29.1	4.2	2483.3
8	28.1	0.8	2706.5
9	37.0	3.0	3409.2
10	29.1	4.4	2483.3
Average	30.1	2.2	2669.9
Standard deviation	6.9	1.3	

Note S2. Calibration for the length of the Si NWs

Equation (3) shows that the resonant frequency (f_i) is highly sensitive to the length (L) of a NW ($f_i \propto 1/L^2$). Thus, the accuracy of the length measurement is an important issue to be taken into account. We carefully corrected the length by considering the systematic error generated by switching the magnifications and the height difference between two ends of a NW (Fig. S1(a),(b),(d)). The magnification error was firstly calibrated by using graphitic lattices at 300k magnification, and then the lower magnification was calibrated by measuring the distance between the two characterized particles at different magnifications. The altitude difference was measured by focusing on the two ends of a NW and recording the defocus difference. The calibration method was applied for every Si NW before a resonance experiment. The actual length (l) was calculated by taking into account the magnification error (e) and altitude difference (ΔH) and is expressed as:

$$l = \left[\left(l_{\mathrm{p}} e\right)^2 + \Delta H^2\right]^{\frac{1}{2}} \tag{S1}$$

where l_{p} is the measured projected length at a low magnification (*e.g.* 12000X) for the resonance experiments.

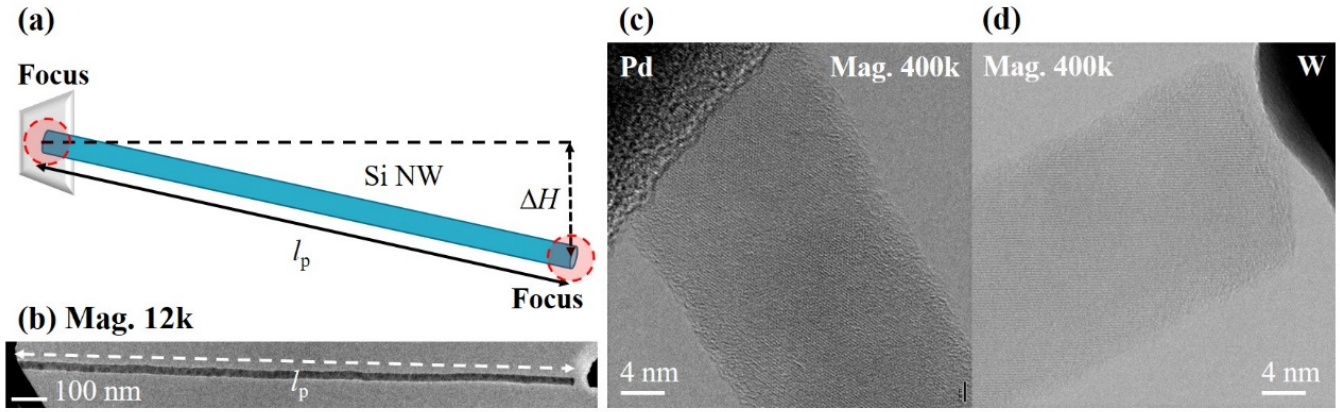

Fig. S1 Calibration for NW length. (a) Schematic illustration of the Si NW altitude difference (ΔH) between the two focal planes marked by red circles on the two ends. (b) The measured projected length (l_p) of the Si NW. (c) Fixed-end side of the Si NW was attached to a Pd electrode edge. (d) Free-end side of the Si NW was slightly touched by the W probe to measure the defocus and altitude difference.

Note S3. Error estimation of defocus for measuring height difference and length

We used the difference of minimum contrast defocuses at both ends to calculate the altitude differences. The contrast transfer function of our microscope (JEOL 3100FEF) is simulated from "contrast transfer function explorer", under the following conditions: voltage 300 kV, Cs 0.6 mm, Cc 1.5 mm, energy spread 0.9 eV, HT ripple 2 ppm, object lens instability 1 ppm. The minimum contrast defocus is about -14 nm. In our experiments, we have changed the defocus back and forth to get the minimum contrast and the maximum error should be ~10 nm. Such an error in altitude measurement will lead to an average error of the length ~0.17%, $\Delta L = ((l_p e)^2+(\Delta H+10)^2)^0.5$ where ΔL is the average length after calibration, l is the average actual length, e is the average magnification error and ΔH is the average altitude difference.

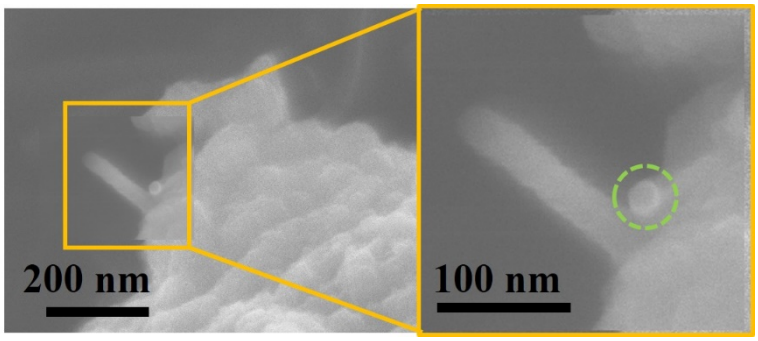

Fig. S2 The SEM image of the circular cross-section of the Si NW.

Note S4. Tungsten probe preparation and SEM morphology

W probes were prepared by electrochemical etching method.[1] A 0.25 mm W wire as an anode was etched by 5M of NaOH solution applied with DC current (Fig. S3(a)). In Fig. S3(b) shows a typical W probe with ~12.6 nm radius of curvature at the apex measured by scanning electron microscope (SEM).

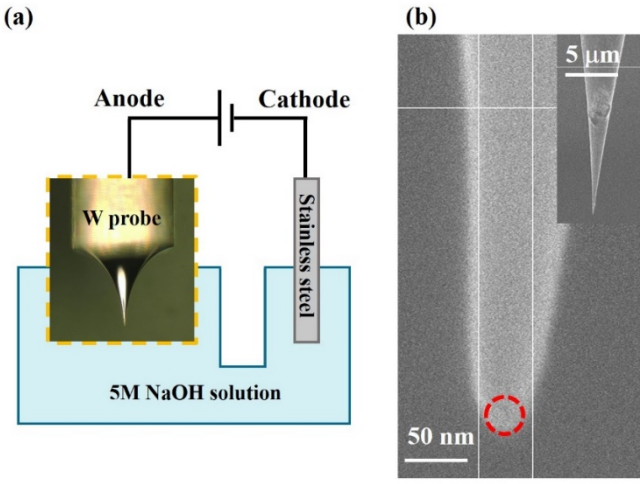

Fig. S3 Tungsten probe preparation setup and morphology. (a) Electrochemical etching preparation setup where a tungsten (W) wire as an anode and stainless steel as a cathode. (b) Scanning electron microscopy (SEM) image shows a typical W probe with ~12.6 nm radius of curvature at the apex marked by red dashed circle.

Note S5. *In situ* TEM measurements of the mechanical resonance

In situ resonance experiments were carried out in a JEOL-3100F TEM operated at 300 kV using a STM-TEM holder ("Nanofactory Instruments AB") with one piezo-controlled W probe and another fixed Pd electrode on which Si NWs were tightly attached using a conductive silver paste. (Fig. 2) A sinusoidal electric signal for inducing mechanical resonance was applied across the two electrodes by a "Tektronix Arbitrary/Function Generator" (AFG3152C), which can provide a peak to peak voltage (V_{pp}) ranging from 1 μV_{pp} to 10 V_{pp} between 1 μHz and 100 MHz, and 1 μV_{pp} to 8 V_{pp} between 100 MHz and 150 MHz. The charge of the Si NW induced by the electric field can be described by: $Q = \alpha(Q_o + e(V_{dc} + v(t)))$, where α is a geometric parameter, Q_o is a static charge from the difference of the work function of two electrodes ($\phi_{Si} - \phi_W$), and V_{dc} is the applied voltage.[2] Here $v(t)$ is the sinusoidal signal $v(t) = V_p \sin(2\pi f_d t)$, with peak voltage $V_p = 0.5V_{pp}$, and driving frequency f_d. The electric force is proportional to the square of the charge described as $F_e = \varphi Q^2$, where φ is a constant.[2] Substituting Q into F_e, the electric force is then given by:[2,3]

$$F_e = \alpha^2 \varphi \left\{ \left[(Q_0 + eV_{dc})^2 + \frac{1}{2} e^2 V_p^2 \right] + \left[2eV_p (Q_0 + eV_{dc}) \right] \cos 2\pi f_d t + \left[\frac{1}{2} e^2 V_p^2 \right] \cos 4\pi f_d t \right\}$$
$$= F_{e0} + F_{e1} \cos 2\pi f_d t + F_{e2} \cos 4\pi f_d t \quad \text{(S2)}$$

The cosine terms indicate the first and the second harmonic modes at f_d and $2f_d$, respectively.[4–6]

Note S6. Application of Mathieu equation in electric-field induced mechanical resonance

In addition to the normal mode resonance, parametric resonance could be induced by a parametric excitation, which can be described as a homogeneous differential equation with periodically varying coefficients. In the case of a single-degree-of-freedom system, the Mathieu equation describes the parametric resonance as:[7]

$$\frac{\partial^2 u}{\partial t^2} + (\delta + \varepsilon \cos 2t)u = 0 \tag{S3}$$

where δ and ε are Mathieu linear and trigonometric parameters, which correlate with a square of the resonant frequency and the oscillation amplitude, respectively. The external force term along with the vibration direction of the equation of motion in Equation (2) equals to a sinusoidal electric force in Equation (S2) written as:[5,8]

$$\rho A(x)\frac{\partial^2 u_i}{\partial t^2} + E_{\text{eff}} I \frac{\partial^4 u_i}{\partial x^4} = \alpha^2 \varphi \left[(Q_0 + eV_{\text{dc}})^2 + \frac{1}{2}e^2 V_{\text{p}}^2 \right.$$
$$\left. + 2eV_p(Q_0 + eV_{\text{dc}}) \cos 2\pi f t + \frac{1}{2}e^2 V_{\text{p}}^2 \cos 4\pi f t \right] u_i \tag{S4}$$

By separation of variables method, $u_i(x,t)$ can be written as:

$$u_i(x,t) = u_i(x) \times u_i(t) \tag{S5}$$

The homogeneous solution of the displacement term of Equation (S4) by substituting equation (S5) is then derived as:

$$\frac{\partial^4 u_i}{\partial x^4} = \beta_i^4 u_i \tag{S6}$$

Combining Equations (S4) and (S6) and rescaling time variables in Equation (S4) to dimensionless values (with ω^{-1}) give the equation of motion as:

$$\frac{\partial^2 u_i}{\partial t^2} + \frac{1}{\omega_n^2}\left(\omega_i^2 + \frac{(Q_0+eV_{\mathrm{dc}})^2+\frac{1}{2}e^2V_{\mathrm{p}}^2}{\rho A} + \frac{2eV_{\mathrm{p}}(Q_0+eV_{\mathrm{dc}})}{\rho A}\cos t + \frac{e^2V_{\mathrm{p}}^2}{2\rho A}\cos 2t\right)u_i = 0 \tag{S7}$$

where $\omega_i^2 = (EI/\rho A)\beta_i^4$, ω_n is parametric angular frequency (n = 1,2,…), and $\delta = \omega_n^{-2}\{\omega_i^2 + [(Q_0 + eV_{\mathrm{dc}})^2 + 1/(2e^2V_{\mathrm{p}}^2)]/\rho A\}$ is the same as the parameter in Mathieu equation (S3), whose solution can be considered as a Fourier series: $u(t) = \sum_{n=1}^{\infty}(a_n cos\ 2nt + b_n sin\ 2nt)$. According to the procedure of harmonic balance, four infinite order determinants (Hill's determinants) can derive the transition curves on δ and ε plane, where parametric resonance occurs (Fig. S4), when:

$$\delta = \frac{n^2}{4} \tag{S8}$$

The relation between parametric frequency and normal mode frequency is associated with Equation (S7) as:

$$\omega_n^2 = (\frac{4}{n^2})\left(\omega_i^2 + \frac{(Q_0+eV_{\mathrm{dc}})^2+\frac{1}{2}e^2V_{\mathrm{p}}^2}{\rho A}\right) \approx \frac{4}{n^2}\omega_i^2 \tag{S9}$$

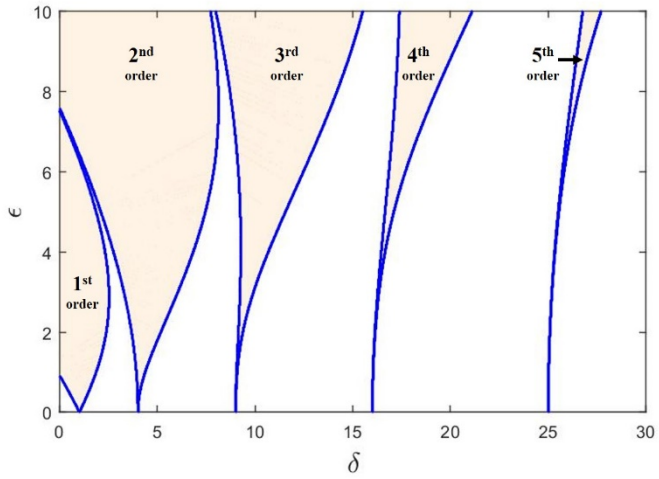

Fig. S4 Strutt diagram visualizing five parametric instability regions of the Mathieu equation. The parametric resonance occurs within the instability region (orange shaded area) bounded within the transition curves (blue curves).

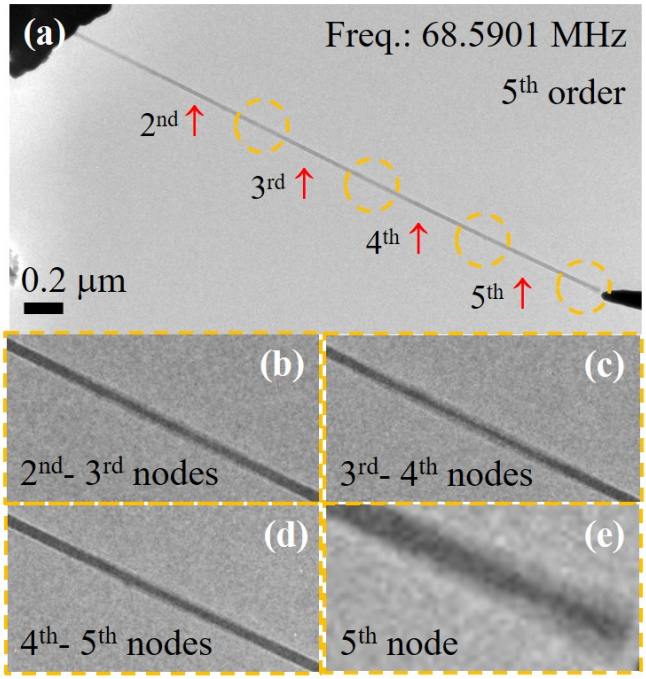

Fig. S5 The zoomed-in images of parametric resonance (n = 4) at the 5th order. (a) The Si NW oscillates at ~68.6 MHz. The red arrows point out four node positions, and four orange dashed circles show oscillating motions between nodes by four zoomed-in images below (b)-(e).

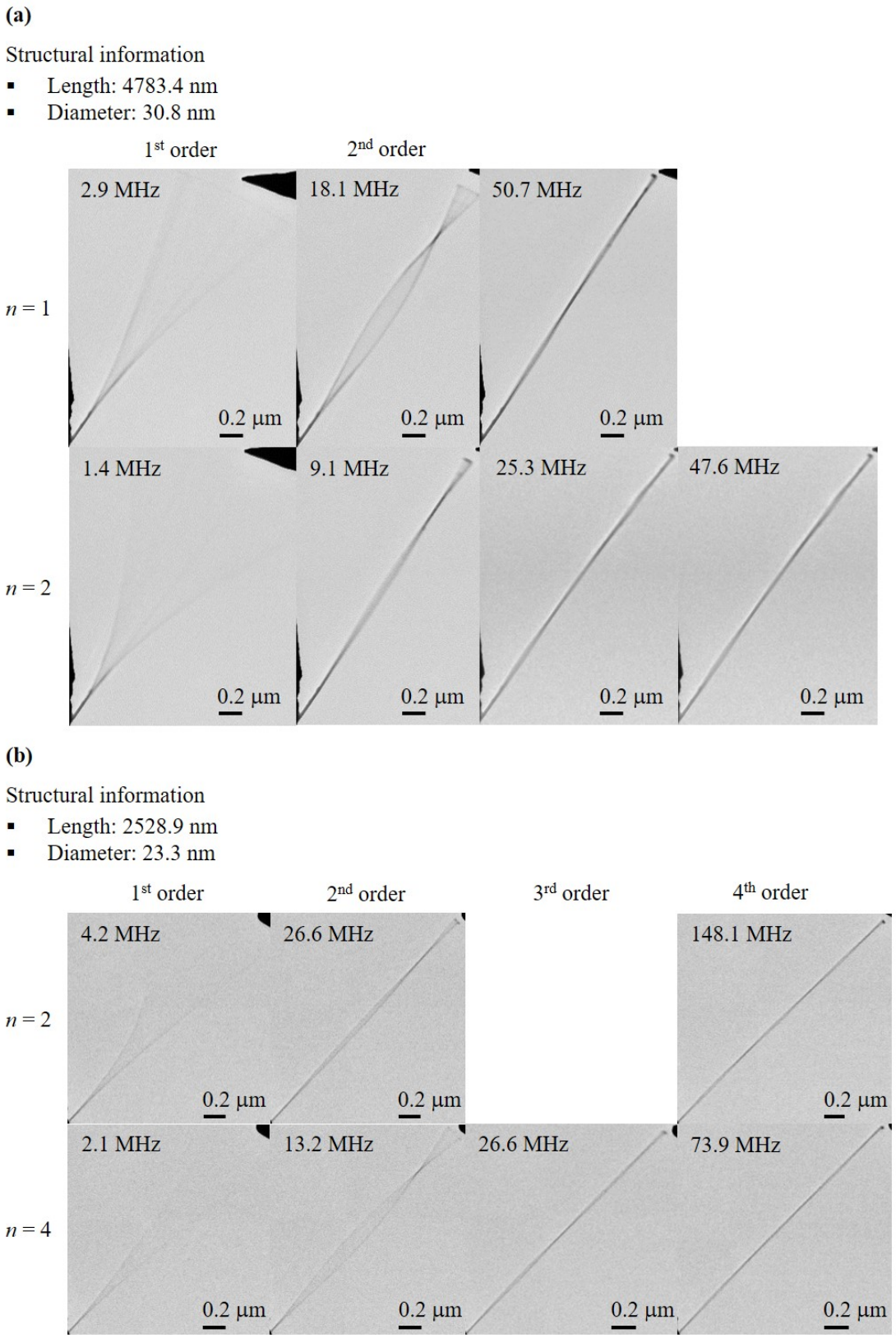

Fig. S6 Resonant orders and parametric modes of two Si NW samples with corresponding resonant frequencies and structural information.

Note S7 Comparison of mode orders for normal and parametric resonances

Based on the Euler-Bernoulli (E-B) beam theory, the ratio between different mode orders at the same parametric mode can be derived from Equation (3) along with a formula:

$$\frac{f_i}{f_j} = \frac{\beta_i^2}{\beta_j^2} \tag{S10}$$

where i and j are the mode order (i, j = 1 ~ 5). Fig. S7 shows the ratio of the normal mode (n = 2), parametric mode (n = 4) and the theoretical calculation (red hollow square) using Equation (S10) from the 1st order to the 5th order based on the 5th order. Comparing the experimental data to the theoretical calculations, the coefficient of determination (R^2) becomes 0.9999 and 0.9997 for n = 2 and n = 4, respectively. The result shows a good agreement with the E-B beam theory, which indicates that such theory can reliably explain the resonant frequency at different mode orders, for both n = 2 and n = 4 resonances.

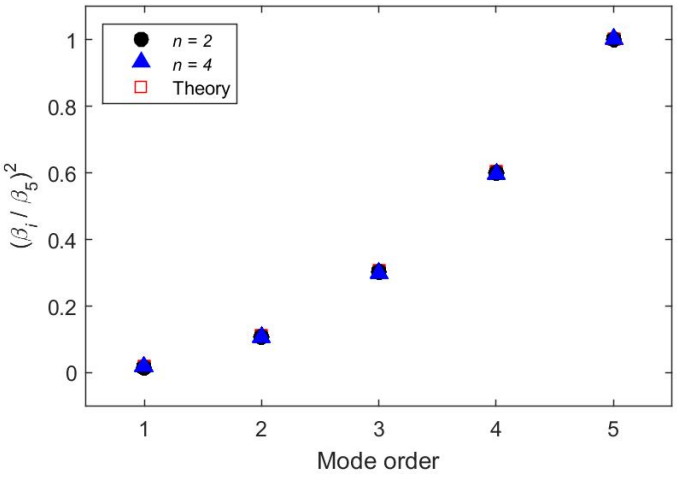

Fig. S7 Comparison of mode orders for normal and parametric resonances.

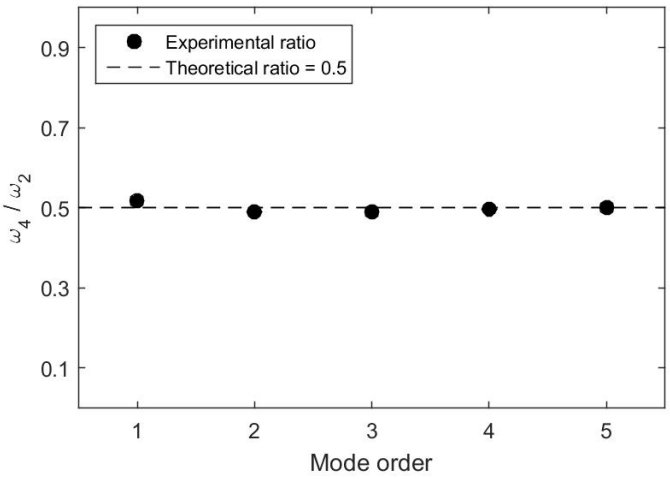

Fig. S8 Comparison of normal ($n = 2$) and parametric resonances ($n = 4$) at different mode orders.

Note S8. Numerical calculations of maximum potential energy of vibrating NW

Based on the principle of conservation of energy, the maximum kinetic energy (T) equals to the maximum potential energy (U_i) stored in the oscillated Si NW at different mode orders. At the maximum vibration amplitude, U_i is expressed as:[9]

$$U_i = \frac{1}{2}\int_o^L M_i d\theta \tag{S11}$$

where M_i is the moment of the deformed NW at different mode orders along the NW length (L) direction, which indicates that the potential energy is the work to deform the NW. According to the E-B beam theory, Equation (S11) is rewritten as:

$$U_i = \frac{1}{2} EI \int_o^L \left(\frac{d^2(u_i(x))}{dx^2}\right)^2 dx \tag{S12}$$

where u_i = (sin$\beta_i x$-sinh$\beta_i x$)-[(sin$\beta_i L$+sinh$\beta_i L$)/(cos$\beta_i L$ +cosh$\beta_i L$)](cos$\beta_i x$ -cosh$\beta_i x$) is the mode shape at different mode orders. Fig. S9 demonstrates the normalized energy at different mode orders by dividing the maximum potential energy at each mode order in Equation (S12) with the maximum potential energy at the 1st mode, U_i/U_1.

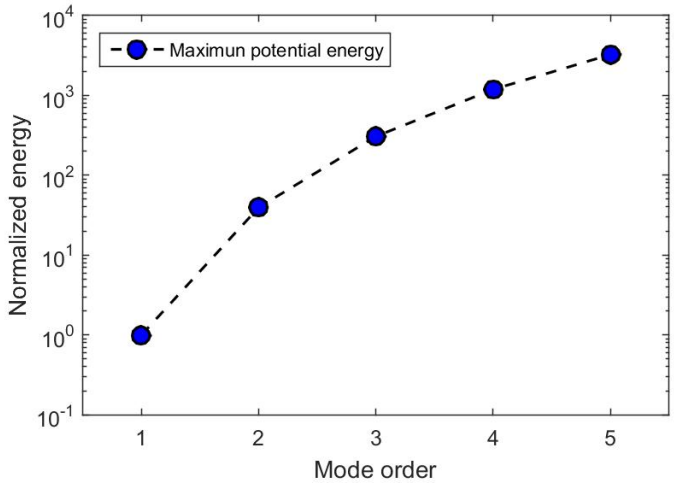

Fig. S9 Numerical calculations of maximum potential energy for five resonant mode orders.

Note S9. Energy dissipation at different mode orders

Under repeated probing of the same Si NW, we observed an increasing trend of the sweeping resolution with increasing the mode order. Such a trend can be explained by the energy dissipation, *i.e.* damping, at the different mode orders. Since *in situ* TEM is operated in a high vacuum (10^{-5} Pa), viscous damping caused by molecules and particles in air could be ignored.[10] The damping mainly contributed by the intrinsic defects and clamping loss of the Si NW.[11–13] Therefore, the damping can be observed as a difference between the input and output energies at the resonant frequency:[14]

$$A_{\mathrm{O}} = \frac{4A_{\mathrm{I}}\omega_i^{\frac{1}{2}}}{\gamma_i}\left(\frac{EI}{\rho AL^4}\right)^{\frac{1}{4}} \tag{S13}$$

where A_{o} is the output amplitude, which is the vibration amplitude of the Si NW, A_{I} is the input amplitude, which is proportional to the electric force, and γ is a damping coefficient. Equation (S13) expresses that the vibration amplitude is proportional to the energy. By substituting the correlation between the resonant frequency and eigenvalue at different mode orders in Equation (3), the damping coefficient can be expressed as:

$$\gamma_i \propto \frac{A_{\mathrm{I}}\beta_i}{A_{\mathrm{o}}} \tag{S14}$$

The normalized damping coefficient is calculated by γ_i/γ_1. Fig. S10 demonstrates that the normalized damping coefficient increases with mode orders, which indicates less energy dissipation at a low-order mode but more at a high-order mode.

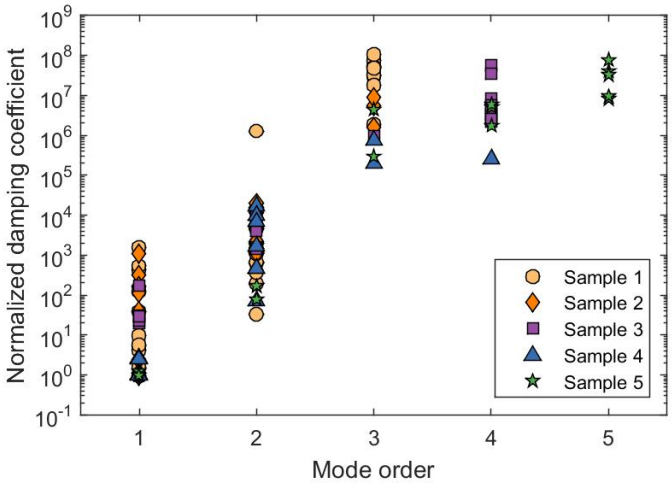

Fig. S10 A normalized damping coefficient increases with the mode order.

Note S10. Limitations of *in situ* observation for higher resonant mode orders

There are intrinsic and extrinsic limits. Intrinsic limit is the crystallinity of the Si NWs, which determines the energy dissipation. In our work, the observed normal and parametric modes up to the 5th order indicates the high quality of the Si NWs. Extrinsic limits include the frequency and power limits of our function generator (Tektronix AFG3152) and also the resolution of the CCD camera. For higher orders, the resonant frequency (f) at different orders (i) increases with the following equation: $f_i \propto \beta_i^2$ where $\beta_i \cong (2i\text{-}1)\pi/2$ (see Equation (3)). Our instrument limits the frequency to 150 MHz. The resonating energy also increases along with the increase of frequency where the dependency between resonating energy and frequency is shown in Fig. 4(a). The voltage of our instrument is limited to 10 V, which limits the vibration amplitude. To observe the resonating shape of the NW, the magnification was set at 6000X. The resolution of the CCD camera at this magnification is ~1.3 nm per pixel.

Note S11. The influence of the catalyst nanoparticle on the calculation of elastic modulus

To investigate the influence of the nanoparticle attached on the free-end of the Si NW to the resonant frequency (f), we employ following equation:[15] $f_o = f_p(1+\Delta m/c)^{0.5}$ where f_o and f_p is the resonant frequency without and with attached nanoparticle, Δm is the mass of the nanoparticle, and c is a geometry constant ($c = \rho AL$ where ρ is the density, A is the area of cross-section and L is the length of the Si NW). For example, the 2nd order resonant frequency attached with a nanoparticle (f_p) of the Si NW is recorded at 26.4667 MHz and the average diameter (d_p) of the Au nanoparticle is 22.2 nm. f_o is derived to be 27.0428 MHz, about 2% changing from f_p. The elastic modulus at the 2nd order based on the E-B beam theory is calculated by following equation: $E_{eff} = \rho(8\pi fL^2/22.0345*d)^2$ (see Equation (7)) where E_{eff} is the effective modulus, f is the resonant frequency at the 2nd order and d is the diameter of the Si NW. The elastic modulus of Si NW with nanoparticle (E_p) is calculated with f_p and l where $l = l_{si} + l_p$ is the length of Si NW (l_{si}) and nanoparticle (l_p). And the elastic modulus without nanoparticle (E_o) is calculated with f_0 and l_{si}, about 0.77% changing from E_p.

Table S2. Comparison of the ratio of node positions (x) to a NW length (L), x/L, between numerical calculations and experimental results; the relative errors at different mode orders are also shown.

		Node 2	Node 3	Node 4	Node 5
Numerical calculation	Mode 2	0.78			
	Mode 3	0.50	0.87		
	Mode 4	0.36	0.64	0.91	
	Mode 5	0.28	0.50	0.72	0.93
Experimental results $n = 2$	Mode 2	0.79			
	Mode 3	0.50	0.88		
	Mode 4	0.34	0.64	0.93	
	Mode 5	0.26	0.50	0.74	0.94
Relative error (%) $n = 2$	Mode 2	0.33			
	Mode 3	1.18	1.03		
	Mode 4	4.34	0.98	2.33	
	Mode 5	4.94	0.38	1.87	1.27
Experimental results $n = 4$	Mode 2	0.79			
	Mode 3	0.48	0.91		
	Mode 4	0.34	0.64	0.92	
	Mode 5	0.27	0.50	0.73	0.94
Relative error (%) $n = 4$	Mode 2	0.29			
	Mode 3	4.58	4.62		
	Mode 4	5.51	0.80	1.72	
	Mode 5	4.75	0.12	1.09	1.28

Video S1

A video showing five orders of the normal mode recorded under *in situ* TEM.

References

S1 M. Setvín, J. Javorský, D. Turčinková, I. Matolínová, P. Sobotík, P. Kocán and I. Ošťádal, *Ultramicroscopy*, 2012, **113**, 152–157.

S2 X. Bai, E. G. Wang, P. Gao and Z. L. Wang, *Nano Lett.*, 2003, **3**, 1147–1150.

S3 K. H. Liu, W. L. Wang, Z. Xu, L. Liao, X. D. Bai and E. G. Wang, *Appl. Phys. Lett.*, 2006, **89**, 221908.

S4 K. Yum, Z. Wang, A. P. Suryavanshi and M.-F. Yu, *J. Appl. Phys.*, 2004, **96**, 3933–3938.

S5 Y. Shi, C. Q. Chen, Y. S. Zhang, J. Zhu and Y. J. Yan, *Nanotechnology*, 2007, **18**, 075709.

S6 R. Gao, Z. L. Wang, Z. Bai, W. A. de Heer, L. Dai and M. Gao, *Phys. Rev. Lett.*, 2000, **85**, 622–625.

S7 A. H. Nayfeh and D. T. Mook, *Nonlinear oscillations*, John Wiley & Sons, 2008.

S8 M.-F. Yu, G. J. Wagner, R. S. Ruoff and M. J. Dyer, *Phys. Rev. B*, 2002, **66**, 073406.

S9 S. S. Rao and F. F. Yap, *Mechanical vibrations*, Prentice Hall Upper Saddle River, 2011, vol. 4.

S10 J. E. Sader, J. Lee and S. R. Manalis, *J. Appl. Phys.*, 2010, **108**, 114507.

S11 J. H. Ko, J. Jeong, J. Choi and M. Cho, *Appl. Phys. Lett.*, 2011, **98**, 171909.

S12 M. K. Ghatkesar, V. Barwich, T. Braun, J.-P. Ramseyer, C. Gerber, M. Hegner, H. P. Lang, U. Drechsler and M. Despont, *Nanotechnology*, 2007, **18**, 445502.

S13 M. Imboden and P. Mohanty, *Phys. Rep.*, 2014, **534**, 89–146.

S14 C. E. Repetto, A. Roatta and R. J. Welti, *Eur. J. Phys.*, 2012, **33**, 1187–1195.

S15 R. Chowdhury, S. Adhikari and J. Mitchell, *Phys. E Low-dimensional Syst. Nanostructures*, 2009, **42**, 104–109.